Cloud Imager Requirement Analysis for the Copernicus CO₂ Monitoring mission

Jochen Landgraf

SRON Netherlands Institute for Space Research, Utrecht, The Netherlands

Abstract:

This Technote summarizes basic analyses to derive a set of requirements for the cloud image CLIM of the Copernicus CO_2 monitoring mission CO2M. Requirements are provided for the band selection in the visible and shortwave infrared, the signal-to-noise performance and the spatial resolution and sampling of the observations. Overall, requiring that at least a 5 % coverage of a 2x2 km^2 spatial sampling of the CO2I spectrometer with cloud must be detectable by the cloud imager, a spatial resolution and sampling $<400 \times 400$ m^2 is required. Moreover, the spectral sizing of the imager must include two spectral band at 550 nm and 1.37 μm with a spectral band width of 20 nm and 15 nm, respectively. Here, one may consider to replace the 550 nm band with a corresponding band at 670 nm, given advantages for cloud detection over vegetation surfaces. The required SNR is 200 for both the 550 nm and 1.37 μm with a radiance reference value of 58.24 and 13.4 mW/(m^2 nm sr), respectively.

Table of Contents

1   Introduction

To infer XCO_2 and XCH_4 dry air column mixing ratios from radiance spectra of shortwave infrared spectrometers, cloud clearing of the observation data set is requested. In the context of the CO2M mission, the challenging accuracy requirements with an XCO_2 accuracy ≤ 0.5 ppm and a XCH_4 accuracy ≤ 10 ppb [Meijer et al., 2020] means very strict cloud filtering, which can only be realized using multiple types of measurements. For this purpose, a cloud image (CLIM) is an important mission payload, which is complemented by observations of the multiangle polarimeter (MAP), and the spectrometer (CO2I). Here, CO2I observations of the O_2 A band can be used to filter major cloud contamination and simultaneous spectral measurements in a weak and strong absorption band of both CO_2 and H_2O can be used to filter on the presence of elevated, optically thin scattering layers. It is shown in serval studies that the cloud clearing approach using radiance observations in the O_2 A and strong and weak absorption bands of CO_2 and H_2O is valuable for the data processing of NASA's OCO-2 and JAXA's GOSAT mission [e.g. Taylor et al. 2016]. For the GOSAT mission complementary observations of the cloud imager are available, which are employed for cloud clearing by the operational processor. For the TROPOMI XCH_4 processing of the Copernicus Sentinel 5 Precursor mission with moderate spectral resolution, it is essential to use collocated VIIRS imager data for cloud clearing [Lorente et al., 2020]. Considering these experience with operational greenhouse gas missions, we advise to base the CO2M cloud clearing on observations of the spectrometer CO2I, the polarimeter MAP and in particular on dedicated measurements of the cloud imager CLIM.

This document derives requirements of a simple two-band imager with high spatial sampling to detect fractional cloud coverage within a 2x2 km^2 pixel area of a CO2I spatial sampling. It must include one spectral band around 550 nm to use the radiometric contrast between clouds and clear sky scenes for cloud detection and one spectral band at 1.37 μm with very strong water vapour absorption to detect the presence of optically thin cirrus. Overall, this document is structured as follows: Section 2 summarizes the high error sensitivity of a full-physics XCO_2 product regarding the presence of clouds in the observed scene, where we employ the spectral sizing of the CO2I instrument as proposed in Meier et al., 2020. The analysis is based on the RemoTeC algorithm and synthetic measurement simulation. Here, the RemoTeC software package is the baseline of the operational S5P and S5 processing and is successfully used to infer XCO_2 and XCH_4 from GOSAT and OCO-2 data. Section 3 indicates the basic elements of the XCH4 cloud clearing approach for S5P. Although the TROPOMI instrument with the 2.3 μm band differs in its spectral sizing and mission objectives significantly from the required CO2I instrument, its operation in loose formation with the VIIRS imager can guide us in the definition of the CLIM imager. Finally, Section 4 and 5 addresses requirement of the CLIM instrument regarding spatial sampling and the spectral band definition using basic analysis. The proposed CO2M CLIM requirements are summarized in Section 6.

2   Cloud error sensitivity of the CO2M XCO₂ product

This section illustrates the large error sensitivity of the XCO_2 product with regard to the presence of clouds in the observed scene. Therefore, we perform XCO_2 retrievals employing the RemoTeC algorithm [e.g. Butz et al., 2009, 2011] for the proposed spectrometer spectral sizing point of CO2I [Landgraf et al., 2020]. We consider a broken field of altocumulus clouds at an altitude of 2 km, where we describe the top-of atmosphere radiance by the independent pixel approximation,

$$I = (1 - f_{cld})I_{clr} + f_{cld}I_{cld}.$$

Here, I_{clr} and I_{cld} are radiance spectra for a clear sky and fully cloudy scene and f_{cld} is the cloud fraction. Obviously, this approximation ignores any three-dimensional effect of radiative transfer but is sufficient for our analysis. For the simulation, we assume a Lambertian surface albedo of $A_{NIR} = 0.2$, $A_{SWIR1} = 0.1$ and $A_{SWIR2} = 0.05$ in the three spectral fit windows. For the cloudy scene, radiances are calculated for a cloud of an optical thickness of 20, which corresponds to a typical Lambertian albedo of 0.6. Figure 2-1 indicates that this cloud induces unacceptable large error on the XCO_2 column depending on the cloud fraction. Already for $f_{cld} = 0.05$, the XCO_2 error exceeds 50 ppm, which is non-compliant by a factor of 100.

Main reason for the large XCO_2 biases is the fact that clouds change the light path and shield the atmosphere below. So, spectrometer measurements from space are not sensitive to the amount of CO_2 below the cloud, leading to the underestimation of XCO_2 in the retrieval. Here, the brightness difference between clear sky and cloudy scene is of little relevance as it is demonstrated in Fig. 2-2. Instead of mixing a clear sky and cloud scene, we considered in this figure the weighted sum of two clear sky scenes with different surface albedo, the Tropical Dark and Tropical Bright reference scene as defined by Meier et al. 2020, namely

$$I(\lambda) = (1 - a)I_{TD}(\lambda) + aI_{TB}(\lambda)$$

Here the mixing factor a corresponds to the cloud fraction f_{cld} in Eq. (1). For a non-scattering atmosphere, the light path for both scenarios is the same and the radiative transfer is a linear function of the surface albedo. This means that the weighted sum in Eq. (2) can be described by a corresponding average of the surface albedo without any loss of accuracy. So, for a non-scattering retrieval, no bias is induced by this mixing of clear sky scenes. Obviously, due to atmospheric scattering by aerosols and air molecules, the dependence of the top of atmosphere radiance on surface albedo is more complex and can only be approximated to be linear. Figure 2-2 shows that this brightness contrast within a scene causes only small errors < 0.1 ppm.

Overall, we conclude that cloud induced errors are significant and that observations with any cloud contamination must be filtered out completely by the CO2M data processing.

3   TROPOMI cloud filtering

The TROPOMI spectrometer on the Sentinel 5 Precursor satellite flies in loose formation with the SUOMI-NPP satellite having the VIIRS cloud imager aboard. The S5P operation processor spatially collocates VIIRS data to TROPOMI SWIR soundings, given a VIIRS cloud fraction for each TROPOMI measurement. Due to the short time difference of < 5 min, it is fair to assume that both the TROPOMI observations and VIIRS data are temporal collocated. SWIR data are only processed if the VIIRS cloud fraction f_{cld} for the TROPOMI target pixel and the eight adjacent pixels is below a threshold ($f_{cld} < 0.001$). Here, this strict cloud clearing of the data is required to achieve the envisaged XCH4 accuracy < 1 % (18 ppb), but leads to a reduced XCH_4 data yield of 10-15 % of all observations. Figure 2-1 shows an example of a XCH_4 emission plume released by an oil and gas production facility close to the city Mary in East Turkmenistan. The effect of the cloud clearing can be clearly seen for the broken cloud field in the North-East of the zoom-in. Here, TROPOMI cannot provide XCH_4 data with the required accuracy and based on the VIIRS observations data are not processed for this area.
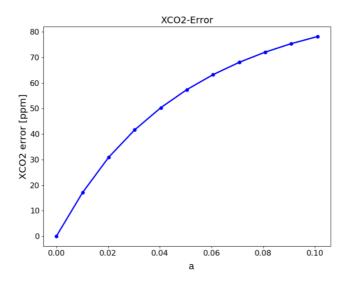
Figure 3-1 XCO₂ error sensitivity as a function of cloud coverage for a scene which is partially covered by a cloud of an optical thickness $\tau_{cld} = 20$ at as cloud height of 2km.
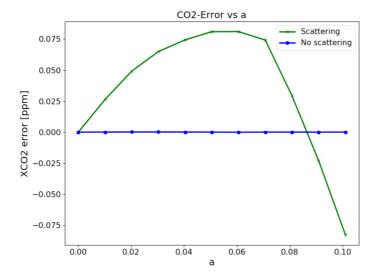

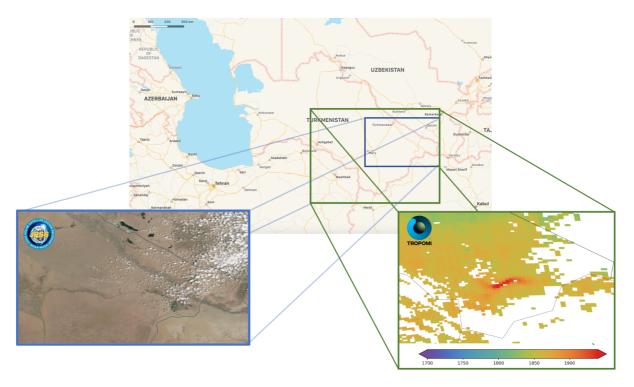*Figure 3-2 Error sensitivity to surface albedo variability within one CO2I ground pixel.*

Figure 3-3 VIIRS cloud filter and TROPOMI data yield for an overpass over East Turkmenistan. The left zoom-in shows an RGB image with a broken cloud field the North-East of the area. Based on the imager information, TROPOMI data are not processed for cloudy observations. Data gaps in the Southern part of the TROPOMI zoom-in are due to other criteria of the S5P XCH4 data quality filtering.

Taylor et al. 2016 proposed a cloud screening algorithm for the OCO-2 data processing, based on independent estimates of the CO_2 column abundances (IEC) using observations taken at 1.61 μm (weak CO_2 band) and 2.06 μm (strong CO_2 band), while neglecting atmospheric scattering. The CO_2 column retrieved from spectral windows with strong and weak telluric absorption of the same trace gas differ significantly in the presence of clouds and so the difference in both columns indicate the presence of clouds. Complementary to this, clouds can be also detected by comparing the surface pressure retrieved from spectral measurements in the 760 nm O_2 A band with a forecast. Based on a combination of both approaches, the OCO-2 cloud clearing approach was successfully validated with collocated MODIS and CALIOP observations.

Using the same concept, a corresponding IEC cloud clearing algorithm was tested for the XCH_4 data processing of S5P. Here, strong and weak CH_4 and H_2O absorption bands were identified in the 2.3 μm as indicated in Fig. 3-2 and a non-scattering retrieval is applied to the corresponding fitting windows. The non-scattering methane column, which is inferred from the weak absorption, exceeds the corresponding column retrieved from a strong absorption band depending on cloud coverage. Figure 3-3 depicts this difference using the strong CH_4 absorption at 2363-2373 nm and the weak absorption at 2310-2315 nm. The figure indicates that the methane two-band retrieval is well suited to detect cirrus cloud even above bright surfaces. Figure 3-4 shows that the same but applied to H_2O absorptions. Compared to CH_4, H_2O absorption lines are narrower, resulting in a different sensitivity towards pressure broadening close to the surface. The H_2O two-band cloud filter is set up analogous to the CH_4 two-band cloud filter. Here, the window 2329-2334 nm contains weak H_2O absorption and the window 2367-2377 nm includes strong H_2O absorption features.

Although simulations indicated that the IEC approach is suited for cloud clearing of S5P XCH4 data, the evaluation of the cloud clearing approach with collocated VIIRS observations showed non-sufficient performance, leading to additional XCH$_4$ biases due to false-positive detection of clear-sky scenes. Reason for the classification errors of this detection scheme is most likely the specific sizing point of TROPOMI, the moderate spectral resolution of 0.25 nm in the SWIR-3 band and the strong interference of the different absorption features in the 2.3 μm spectral range. Therefore, the cloud clearing approach based on VIIRS is chosen as baseline and the IEC approach as a backup option.
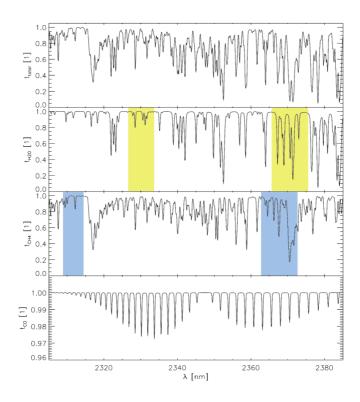

Figure 3-4 Transmission spectrum for the 2.3 μm band of TROPOMI with a spectral resolution of 0.25 nm and the contribution of the different telluric absorbers: H2O (second from top), CH4 (third from top) and CO (bottom). The green areas indicate the strong and weak water vapor absorption bands and the blue areas the corresponding bands of methane.
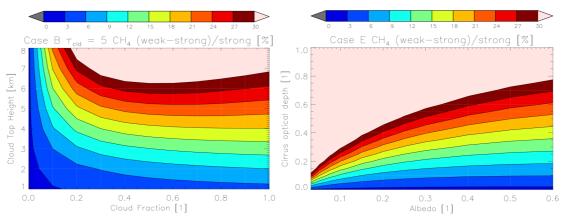
Figure 3-5 CH₄ two-band cloud filter. The methane cloud filter relies on non-scattering methane column retrieval from strong and weak absorption features at 2363-2373 nm and 2310-2315 nm, respectively. The left panel shows the column differences for a water cloud with optical thickness of 5 as a function of cloud height and cloud fraction and the right panel for a cirrus cloud at 10 km height as a function of surface albedo and cirrus optical thickness. (Figure 48 from Landgraf et al., 2018).
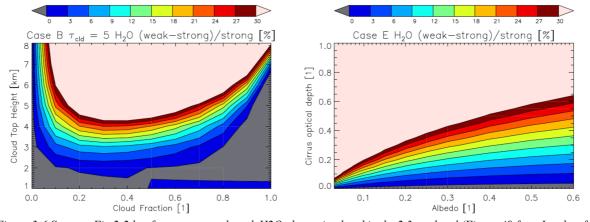

Figure 3-6 Same as Fig 2-2 but for a strong and weak H2O absorption band in the 2.3 µm band (Figure 49 from Landgraf et al., 2018).

In addition to the data filtering based on VIIRS cloud fraction, the processor has the option to evaluate the cirrus reflectance as measured by the M9 channel of VIIRS (1.37 μm). Figure 3-7 shows an example of VIIRS cirrus reflectance around Indonesia. The high reflectance values indicate convective cloud systems with high cloud top height, whereas values close to zero can be used to identify TROPOMI measurements in absence of high clouds. S5P cloud clearing using this quantity as an additional cloud indicator is currently under investigation.

Based on the S5P experience, we recommend to add a cloud imager to the CO2M payload and to base the cloud clearing approach and several indicators such as the cloud fraction derived from imager data and the ICE approach using spectrometer observations.

Figure 3-7: Cirrus reflectance derived from the M9 VIIRS 1.37 μm band collocated with the TROPOMI SWIR pixels.

4   Cloud detection on radiometric contrast of a single band

The previous section indicated that cloud clearing with the required rigor is challenging and requires several quantities to indicate the presence of clouds. For the CO2M mission, we propose to follow a stepwise classification process, where a cloud image is used for a first clearing of the dataset followed by a further analysis using MAP and CO2I observations. This stepwise approach is beneficial as cloud clearing using the imager data is little time consuming and can easily be used to preselect observations in the processor chain.

We start our analysis requiring that a cloud imager CLIM must be capable to detect/classify
   1. cloudy CO2I observations with at least 5 % of the 2x2 km^2 CO2I spatial sampling covered by optically thick clouds ($\tau_{cld} \geq 5$ at an altitude of 2 km).
   2. subvisible cirrus with $\tau_{cir} \geq 0.05$ using a dedicated spectral band at 1.37 μm.

To be compliant with the first requirements, we assume a single channel imager in the visible between 500 and 700 nm and a cloud detection scheme, which is based on the radiometric contrast between the land surface and clouds. Figure 4.1 shows an estimated cloud albedo calculated with a two-stream radiative transfer model. For a cloud optical depth of $\tau_{cld} = 20$ the Lambertian cloud albedo is about $A_{cld} = 0.6$ with some variation due to different illumination at the cloud top, where we consider a solar mean with different illumination angle and isotropic diffuse illumination. For a cloud optical depth of $\tau_{cld} = 5$ the correspondent Lambertian cloud albedo is about $A_{cld} = 0.3$.
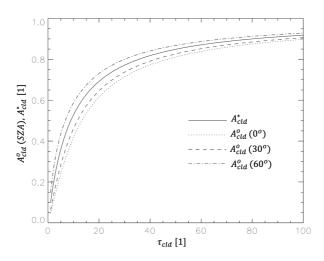
Figure 4-1 Cloud albedo for illumination with direct sun light only $A^o_{cld}(SZA)$ for different solar zenith angle (SZA) and for the illumination with diffuse light A^*_{cld}.
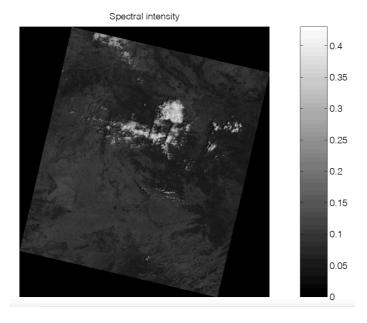

Figure 4-2 radiometric contrast between bright clouds and dark land surface (MERIS R-2003-07-14image, from Gómez-Chova et al., 2005).

For most cases, the clear sky land scenes are darker than surrounding clouds (see Fig 4-2 as an example of a MERIS of a bright cloud over a dark land surface with a spatial resolution of 300 m). Figure 4-3 depicts the spectral dependence of the Lambertian albedo for different surface types. It shows that at 550 nm and 670 nm the surface of sand, soil, vegetation and water with $(A_{sand}, A_{soil}, A_{veg}, A_{water})$=(0.220, 0.107, 0.133, 0.045) and (0.268, 0.167, 0.934, 0.092, 0.030) at 550 and 670 nm, respectively, is significantly darker than a typical water cloud. The figure indicates that for these two bands the contrast between vegetation surface and cloud is largest at 670 nm, whereas for the other surface types it is vice versa and the contrast is largest at 550 nm. As the maximum radiation

intensity of the solar spectrum occurs at 500 nm, we select the 550 nm band as baseline, but consider the 670 nm band as an alternative particular due to its frequent use for the spectral sizing of cloud imagers.

To define requirements for the CLIM instrument, we have to define a reference scene for which certain mission performance aspect must be met. Considering the surface albedo in Fig. 4-3 on one hand and the cloud albedo as a function of cloud optical depth in Fig. 4-1 on the other hand, it is difficult to define a lower limit for cloud albedo for the detection approach. However, it becomes obvious that only clouds with an albedo ≥ 0.3 can be detected over bright sand surfaces (albedo =0.2). This corresponds to an optical thickness of about 5, which we consider as our reference cloud in the following discussion. Next, we have to decide on the cloud height and the fractionation of the cloud field over a CO2I instrument field of view of 2x2 km^2 which is covered by 5 % with clouds. For a CLIM spatial sampling of $N \times N$ pixels within a CO2I field of view, we can assume that each of the CLIM sampling is covered by 5 % with clouds and so we achieve the required 5 % cloud coverage of the CO2I sampling independent on the actual sampling of the imager. Due to the aspired high spatial sampling of the CLIM imager, this means a fragmented cloud field. In this case, the radiometric contrast between clear sky scenes and partially cloudy scenes is little, which yields to strict SNR requirements. In the other extreme, one may assume that 5 % of the CO2I Fovea is covered by one coherent cloud. If this cloud is detected by a single CLIM sounding, it requires a sampling distance of about 450x450 m^2 of the imager. For this case the radiometric contrast between clear sky and cloudy pixel is large. However, this scenario is not likely to happen and so we deem necessary to require a spatial sampling distance of the cloud imager ≤ 400 m (threshold, ≤ 200 m goal) in both horizontal dimensions.
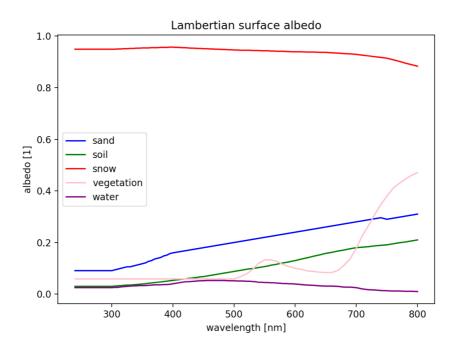

Figure 4-3 Spectral Lambertian surface albedo for five different surface types (see legend). R. Guzzi, private communication.

Next, we make two assumptions to derive the SNR requirement of the 550 nm band of the cloud imager:

1. The CLIM cloudy pixel is covered 5 % by clouds ($f_{cld} = 0.05$) with a cloud albedo $A_{cld} = 0.3$. To identify this cloud coverage corresponds to the most challenging scenario in the discussion above.
2. All clear sky scenes have a vegetation surface with a surface albedo A_{veg}(550nm) = 0.13, for which the contrast between cloud and land surface is large (see Fig. 4-2) and so eases cloud detection.

Ignoring any atmospheric scattering means that the cloudy pixel radiance I_{cld} at the top of atmosphere is proportional to $I_{cld} \propto f_{cld}A_{cld} + (1 - f_{cld})A_{veg}$ i.e.

$$I_{cld} \propto 0.3 \cdot 0.05 + 0.13 \cdot 0.95 = 0.1385.$$

However, for a clear scene holds

$$I_{clr} \propto 0.13$$

Thus, the relative signal enhancement due the cloud is

$$\sigma = \frac{I_{clr}}{I_{cld} - I_{clr}} = 15$$

This number can be compared with a SNR requirement assuming that the SNR must be a factor 5 higher than σ to separate signal from noise, so SNR $\geq$ 75. Analogous, we obtain a required SNR $\geq$ 275 for a sand surface with A_{sand}(550nm) = 0.22. The 5σ confidence level is stringent (99.99994% confidence) and means that in practice we can exclude any statistical error in the cloud clearing due to the SNR performance of the imager. This must hold for all observation geometries covered by the mission performance requirements. To meet the SNR performance $\geq$ 75 and $\geq$ 275 at SZA = 70° means a more stringent SNR requirement at SZA = 50°, which can be estimated by

$$SNR_{sza=50} = SNR_{sza=70}\sqrt{\frac{\cos(50^o)}{\cos(70^o)}}$$

This yields $SNR_{sza=50}$ = 140 and 516 for a vegetation and sand surface, respectively. Obviously, the requirement for sand surfaces is very demanding. As it combines low cloud coverage of individual CLIM pixels with little scene contrast, we consider a $SNR_{sza=50}$ = 200 as an appropriate choice. To simulate the corresponding reference radiance, we consider the geometry SZA = 50° and VZA=0°, the vegetation surface albedo $A_{veg} = 0.13$, and an aerosol-free model atmosphere including Rayleigh scattering by air molecules in the simulations. This leads to a top-of-atmosphere radiance $I_{ref} = 58.24$ mW/(m^2 nm sr), which is very close to the 3MI mission with 55.24 mW/(m^2 nm sr) at 555 nm.

5   Cirrus detection using the 1.37 μm band

Elevated scattering layers even of low optical depth e.g., subvisible cirrus, can induce significant XCO₂ errors. Particular over brighter scenes, multiple scattering of light by cirrus, aerosols and the surface may cause a significant light path enhancement, which is very difficult to account for in a multiband full-physics retrieval of the GOSAT and OCO-2 RemoTeC XCO₂ product. Therefore, XCO₂ data processing must have a mean to filter on the occurrence of cirrus in the observed CO2I scene. Guerlet et al, 2013 proposed the use of GOSAT radiance in the spectral window 1927-1942 nm with saturated water vapor bands. Due to the strong absorption the observed radiance signal diminishes for clear sky observations. However, when light is scattered e.g., by cirrus in the upper troposphere, where the water vapor concentration is low compared to the lower troposphere, a certain fraction of light is scattered into the line of sight of the spectrometer and so a signal is observed even in case of saturated absorption. Figure 5-1 shows the XCO₂ bias as a function of the 'cirrus' signal in the spectral window 1938.8-1940.0 nm, which suggests data clearing using this radiance quantity.

To adapt this approach to the CO2M mission concept would mean a spectral extension of the SWIR-2 spectral window of the CO2I spectrometer, which goes at the cost of a lower spectral resolution (see Landgraf et al., 2020). A more beneficial solution is to add a spectral channel to the cloud imager. Based on MODIS and VIIRS instrument heritage, we propose a spectral band around 1.37 μm in the center of a saturated water band, where the spectral resolution should be wide enough to receive sufficient signal in case of cirrus but also small enough to get not affected by weaker telluric absorptions towards shorter and longer wavelength. The band specification is inspired by the VIIRS design and illustrated in Fig. 5-2.
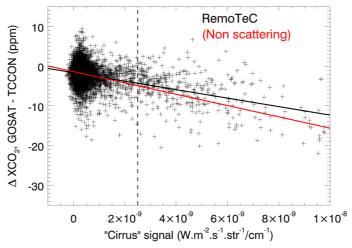

Figure 5-1 GOSAT XCO₂ retrieval bias with respect to collocated TCCON measurements as a function of the mean radiance signal in the range of saturated water vapor 1938.8-1940.0 nm (from Guerlet et al., 2013, Fig. 6).

With the definition of the Gaussian bandpass filter, we can calculate the radiance signal as a function of cirrus optical depth and defining a threshold value for detection leads us than to an appropriated SNR requirement. Figure 5-3 shows the 1.37 μm radiance signal as a function of cirrus optical depth τ_{cir}. For $\tau_{cir} < 0.1$ the radiance signal is small and similar for different SZA. To detect cirrus contamination for $\tau_{cir} > 0.05$, the observation must be sensitive to a radiance signal I>0.1 mW/(m2 nm sr). For a moderate water vapor column, Fig. 5-4 indicates little measurement sensitivity to a changing surface due to the strong H_2O absorption in the band.
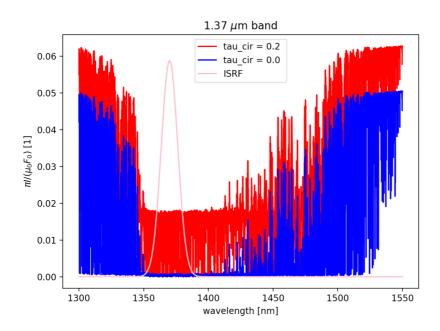
Figure 5-2 Line-by-line reflectance simulations $\pi I/\mu_o F_o$ in the spectral range 1300-1550nm. Simulations are performed for a surface albedo of 0.05, where the cirrus at 10 km altitude is described by a Henyey Greenstein phase function with asymmetry factor g = 0.8. The total H_2O column is 4.75 10^{22} molec./cm². At 1370 nm the water vapor absorption is fully saturated for clear sky conditions. For a cirrus with τ_{cir} = 0.2 and due to light scattering at high altitudes, a clear signal can be recorded in this spectral range. The figure illustrates an appropriate Gaussian bandpass filter with a FWHM=15 nm, which is suited to isolate the signal in the centre of the absorption band from the signal at the band wings.
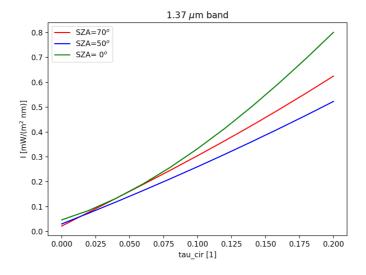

Figure 5-3 1.37 µm radiance as a function of cirrus optical depth for different SZA. Simulations are performed for a moderate water vapor column of 4.75 10^{23} molec./cm² and a surface albedo A_{surf} =0.05.
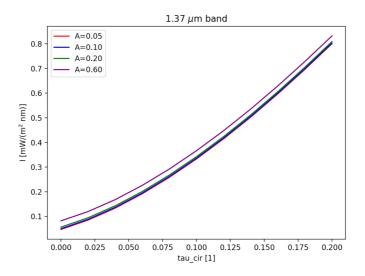
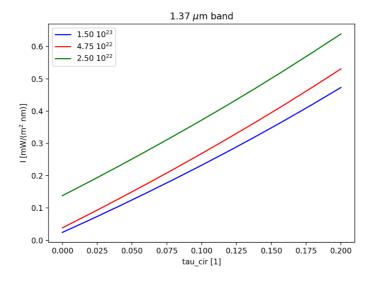*Figure 5-4 Same as Fig 5.2 but for different surface albedo and a fixed SZA =0°.*

Figure 5-5 1.37 μm radiance as a function of cirrus optical depth for a high, moderate and low water vapor column (1.5 10^{23}, 4.75 10^{22}, 2.5 10^{22} molec../cm²) and a bright surface with A_{surf} =0.6 and SZA=50°.

The limitations of this detection approach become clear when we look at the radiance signal for dry air, typically found at elevated areas and higher latitudes. For these conditions in combination with a bright surface, the radiance signal exceeds the indicated threshold value of I_{thresh} =0.1 mW/(m² nm sr) even in the absence of cirrus and so leads to a false negative classification. This means that the data quality is not affects but the data yield is unnecessarily reduced. It remains to be investigated if the MAP may provide a better cirrus detection scheme for these circumstances.

Finally, after motivating the radiance threshold I_{thresh} =0.1 mW/(m² nm sr) it remains to determine a SNR requirement for this channel. We require that the SNR must be high enough to discriminate radiance changes of 0.04 mW/(m² nm sr) with a 5-sigma confidence level. This means that we would like to differentiate a signal of 0.10 mW/(m² nm sr) and 0.14 mW/(m² nm sr) with high confidence. If the measurement error is 0.04 mW/(m² nm sr) then there is a realistic chance of 32 % that the higher

radiance measurements corresponds to a true radiance signal which is below the threshold value. In case of one-fifth of the measurement error (0.008 mW/(m^2 nm sr)), this reduces the uncertainty to 0.00006 %. This corresponds to a SNR of about 20 for I = 0.14 mW/(m^2 nm sr). For the CLIM 1.37 μm channel, the radiometric reference is I_{ref}=9.24 10^{12} ph/(s nm cm2 sr) = 13.4 mW/(m^2 nm sr) in correspondence to other missions (3MI). Assuming a shot noise limited instrument performance, we can scale the SNR to the reference radiance level by

$$\frac{SNR_1}{SNR_2} = \sqrt{\frac{I_1}{I_2}}$$

which yields a SNR = 200 for I_{ref}=13.4 mW/(m^2 nm sr).

6 Summary

After motivating a cloud imager for data screening of the Copernicus CO₂ monitoring mission CO2M, this document yields a set of key requirements for the cloud imager. They are based on the need to detect cloud coverage ≥ 5% of a CO2I spatial sampling and to detect subvisible cirrus of small optical depth ($\tau_{cir} \geq 0.05$). The requirements are

CLIM-1	The spatial resolution and sampling of the CLIM must be < 400×400 m^2 (threshold, 200×200 m^2)

CLIM-2	The CLIM must include a radiance band at 550 nm with a spectral band width of 20 nm[1]

[1]Alternatively, one can consider to use a radiance band at 670 nm where the reference value of the corresponding SNR requirement has to be adjusted accordingly.

CLIM-3	The 550 nm band must achieve a SNR=200 for $I_{ref} = 58.24$ mW/(m^2 nm sr)

CLIM-4	The CLIM must include a radiance band at 1.37 μm with a spectral band width = 15 nm

CLIM-5	The 1.37 μm band must achieve a SNR=200 for $I_{ref} = 13.4$ mW/(m^2 nm sr)

For the cloud clearing of the CO2M observations, we recommend to consider a sequential approach of different filter techniques, where cloud filtering using the CLIM observations should be considered as an initial step. Although requirements were derived on basic radiometric contrast considerations, for the data processing more advanced techniques like data classification using machine learning techniques are recommended. Using spatial correlations of the radiometric contrast may improve the performance of the detection algorithm.
Finally, cloud filtering based on the spectrometer observations are required as well as part of the CO2M processing chain. Here techniques are already well developed and tested for the data processing of the GOSAT and OCO-2 mission. Although the polarimetric measurements may provide very valuable information on cloud coverage, the algorithm development regarding a CO₂ monitoring mission is still at the very beginning and requires more effort to become functional and optimized for the CO2M data processing.

References

Meijer et al., 2020, Copernicus CO2 Monitoring Mission Requirements Document, EOP-SM/3088/YM-ym, issue 3.0, date of issue 01-10-2020.

Taylor, T. E., O'Dell, C. W., Frankenberg, C., Partain, P. T., Cronk, H. Q., Savtchenko, A., Nelson, R. R., Rosenthal, E. J., Chang, A. Y., Fisher, B., Osterman, G. B., Pollock, R. H., Crisp, D., Eldering, A., and Gunson, M. R.: Orbiting Carbon Observatory-2 (OCO-2) cloud screening algorithms: validation against collocated MODIS and CALIOP data, Atmos. Meas. Tech., 9, 973–989, https://doi.org/10.5194/amt-9-973-2016, 2016.

Lorente, A., Borsdorff, T., Butz, A., Hasekamp, O., aan de Brugh, J., Schneider, A., Hase, F., Kivi, R., Wunch, D., Pollard, D. F., Shiomi, K., Deutscher, N. M., Velazco, V. A., Roehl, C. M., Wennberg, P. O., Warneke, T., and Landgraf, J.: Methane retrieved from TROPOMI: improvement of the data product and validation of the first two years of measurements, Atmos. Meas. Tech. Discuss. [preprint], https://doi.org/10.5194/amt-2020-281, accepted for publication, 2020.

Butz, A., O. P. Hasekamp, C. Frankenberg, and I. Aben (2009), Retrievals of atmospheric CO 2 from simulated space-borne measurements of backscattered near-infrared sunlight: accounting for aerosol effects, Appl. Opt., 48, 3322, doi: 10.1364/AO.48.003322.

Butz, A., S. Guerlet, O. Hasekamp, D. Schepers, A. Galli, I. Aben, C. Franken- berg, J.-M. Hartmann, H. Tran, A. Kuze, G. Keppel-Aleks, G. Toon, D. Wunch, P. Wennberg, N. Deutscher, D. Griffith, R. Macatangay, J. Messerschmidt, J. Notholt, and T. Warneke (2011), Toward accurate co2 and ch4 observations from GOSAT, Geophysical Research Letters, 38(14), n/a–n/a, doi:10.1029/2011GL047888, l14812.

Landgraf et al., 2020, Study on Spectral Sizing for CO2 Observations: Tech-Notes. Version 1.1, SRON-CSS-TN-2020-003, issue date: 30-Nov-2020

Landgraf et al., 2018, Algorithm Theoretical Baseline Document for Sentinel-5 Precursor: Carbon Monoxide Total Column Retrieval, issue 1.10. SRON-S5P-LEV2-RP-002

Guerlet, S., A. Butz, D. Schepers, S. Basu, O. P. Hasekamp, A. Kuze, T. Yokota, J.-F. Blavier, N. M. Deutscher, D. W. T. Griffith, F. Hase, E. Kyro, I. Morino, V. Sherlock, R. Sussmann, A. Galli and I. Aben, 2013, Impact of aerosol and thin cirrus on retrieving and validating XCO₂ from GOSAT shortwave infrared measurements, J. Geophys. Res., doi: 10.1002/jgrd.50332